Pergamon

Int. J. Solids Structures Vol. 35, Nos 34–35, pp. 4945–4962, 1998

Printed in Great Britain
0020–7683/98/$—see front matter

PII: S0020–7683(98)00103–6

EFFECTS OF FIXED CHARGES ON THE STRESS–RELAXATION BEHAVIOR OF HYDRATED SOFT TISSUES IN A CONFINED COMPRESSION PROBLEM

V. C. MOW,† G. A. ATESHIAN, W. M. LAI and W. Y. GU
Orthopaedic Research Laboratory, Departments of Mechanical Engineering and Orthopaedic Surgery, Columbia University, New York NY 10032, U.S.A.

(*Received* 24 *September* 1997; *in revised form* 12 *February* 1998)

Abstract—The 1-D confined-compression stress–relaxation behavior of a charged, hydrated-soft tissue was analyzed using the continuum mixture theory developed for cartilage (Lai *et al.*, 1991). A pair of coupled nonlinear partial differential equations governing the displacement component u^s of the solid matrix and the cation concentration c^+ were derived. The initial-boundary value problem, corresponding to a ramp–displacement stress–relaxation experiment was solved using a finite-difference method to obtain the complete spatial and temporal distributions of stress, strain, interstitial water pressure (including osmotic pressure), ion concentrations, diffusion rates and water velocity within the tissue. Using data available in the literature, it was found that: (1) the equilibrium aggregate modulus of the tissue (as commonly used in the biphasic theory) consists of two components: the Donnan osmotic component and the intrinsic matrix component, and that these two components are of similar magnitude. (2) For the rate of compression of 10% in 200 s, during the compression stage, the fluid pressure at the impermeable boundary supports nearly all the load, while near the free-draining boundary, both the matrix stiffness and the fluid pressure support a substantial amount of the load. (3) Equivalent aggregate modulus and equivalent diffusive coefficient used in the biphasic theory can be found, which predict essentially the same stress relaxation behavior. These equivalent parameters for the biphasic model embody the FCD effect of the triphasic medium. The internal fluid pressure predicted by the two models are however different because of osmotic effects. (4) Peak stress at the end of the compression stage is higher for a tissue with higher FCD. We have obtained the strain, stress, flow, pressure and ion concentration fields inside the tissue. Some representative results of these fields are presented. These fields are essential for determining the local variations of mechanical, electrical and chemical environments around cells necessary for the understanding of the mechano-electrochemical signal transduction processes required for the control of biologic functions.

NOMENCLATURE

c^F	fixed charge density
c^α	molar concentration of αth ionic species ($\alpha = +, -$)
D^α	diffusivity of αth ionic species
e	dilatation of solid phase
$\mathbf{E}$	infinitesimal strain tensor
$f_{\alpha\beta}$	frictional coefficients between α and β phases (or constituents)
F_c	Faraday constant
h	thickness
I	electrical current density
$\mathbf{I}$	identity tensor
M^α	molar weight of αth ionic species
p	pressure
R	universal gas constant
T	absolute temperature
v^α	velocity of αth constituent ($\alpha = s, w, +, -$)
γ_α	activity coefficient of αth ionic species
λ_s	Lamé coefficient
μ_s	shear modulus
μ^w	chemical potential of water
μ_0^α	reference chemical potential of αth constituent
$\tilde{\mu}^\alpha$	electrochemical potential of αth ionic species

† Author to whom correspondence should be addressed. 630 West 168th Street, BB1412, Orthopaedic Research Laboratory, Columbia University, New York NY 10032, U.S.A. Tel.: 001 212 305 7965. Fax: 001 212 305 2741. E-mail: mow@cuorma.orl.columbia.edu

ρ^{α}	apparent mass density of αth constituent
ρ_T^{α}	true mass density of αth constituent
σ	Cauchy stress tensor for total mixture
ϕ	osmotic coefficient
φ^{α}	volume fraction of αth constituent
ψ	electric potential
*	quantities associated with external bathing solution

INTRODUCTION

Biological tissues are called charged tissues when their extracellular matrix (ECM) is charged. Articular cartilage, growth plate, invertebral disc, and cornea are examples of charged hydrated soft tissues. The charged nature of the ECM derives from the proteoglycans (PGs) within the tissue. These molecules are very large and have complex macromolecular structures (e.g., Hardingham and Fosang, 1992; Muir, 1983). Each PG molecule (known as an aggrecan) is composed of a single protein core to which are attached glycosaminoglycan (GAG) chains. The dimeric units of these GAGs are usually chondroitin sulfate (CS) and keratan sulfate (KS). At normal physiologic conditions, each dimeric unit of CS has two negative charge groups (SO_3^- and COO^-), and each dimeric unit of KS has one negative charge group (SO_3^-). Thus, each aggrecan is a macromolecular polymer containing numerous negative charged groups, spaced at 10–15 Angstroms apart [Mow *et al.*, 1992; Muir, 1983]. In the tissue, many aggrecans (one to two hundred—depending on age) are attached to a single chain of hyaluronan molecule of approximately 500 kDa. The whole ensemble is known as a proteoglycan aggregate, and its molecular weight can be as high as 200 MDa. In the ECM, the proteoglycan aggregates are entangled within the fine fibrous collagen network to form a strong, cohesive, porous, hydrated ECM (Fig. 1). Relative to the mobile ions (e.g., Na^+, Cl^-) dissolved in the interstitial water, these charges are firmly attached to the ECM, and thus they are called fixed charges. The density of these fixed charges (per volume of interstitial water) is the fixed charge density (FCD).

Within the tissue, the fixed negative charges on the ECM attract mobile cations (mostly Na^+) to maintain electroneutrality at a scale level much greater than the molecular dimensions of CS and KS chains so that the continuum assumption may be used. The electrostatic interactions between fixed charges and mobile ions (at the molecular level) are primarily responsible for many macroscopically observed mechano-electrochemical coupling phenomena, such as the Donnan osmotic pressure, ECM pre-stress, streaming potential, streaming current, negative osmosis, and electro-osmosis (e.g., Akizuki *et al.*, 1986; Buschmann and Grodzinsky, 1995; Eisenberg and Grodzinsky, 1987; Frank and Grodzinsky, 1987; Grodzinsky *et al.*, 1978; Gu *et al.*, 1993, 1997; Lai *et al.*, 1991, 1994;

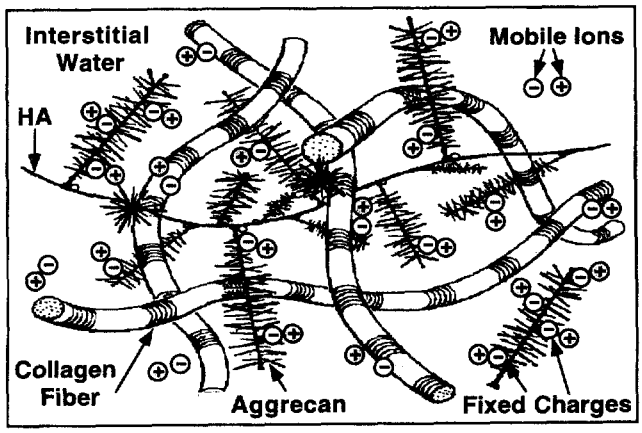

Fig. 1. Schematic of a charged-hydrated soft tissue equilibrated with NaCl solution.

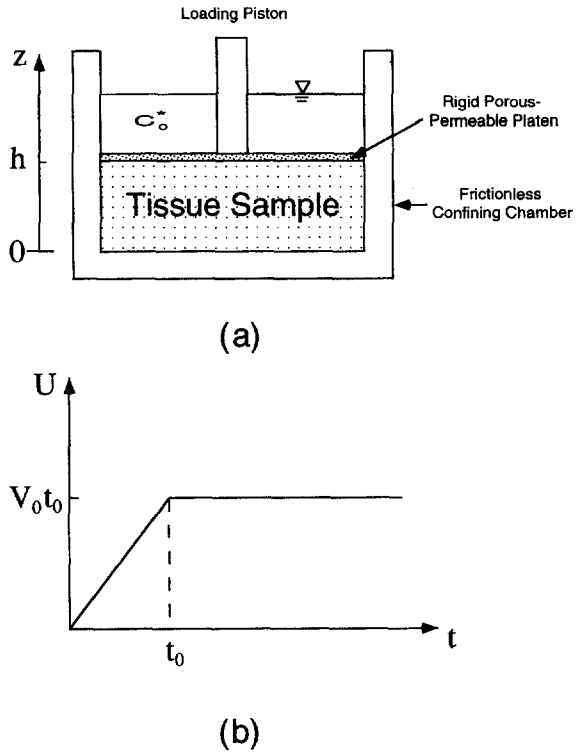

Fig. 2. Schematic of a confined compression stress–relaxation test: (a) the specimen is confined on the lateral surface so that only deformation in the z direction occurs; (b) a ramp displacement is applied at the surface during $0 < t < t_0$. The bathing solution contains 0.15 M NaCl. The specimen chamber is considered to be frictionless, rigid and impermeable.

Katchalsky, 1971; Katchalsky and Curran, 1975; Maroudas, 1979; Mow *et al.*, 1992; Myers *et al.*, 1984; Overbeek, 1956; Setton *et al.*, 1995).

The confined compression stress relaxation tests with porous platens (Fig. 2(a)) have been frequently used for investigating the flow-dependent viscoelastic behavior of biological hydrated soft tissues (e.g., Holmes *et al.*, 1985; Lai *et al.*, 1981; Mow *et al.*, 1980). From the stress–relaxation data, the 1-D compression modulus (i.e., the aggregate modulus) at equilibrium and the hydraulic permeability of the tissue can be calculated using either poroelastic theory developed by Biot (1941) or continuum mixture theory, i.e., the biphasic theory for cartilage developed by Mow *et al.* (1980). In spite of the fact that both theories can predict well the confined compression stress–relaxation experiments (Fig. 2(b)), neither of the two theories, however, account for the swelling pressure effect associated with the FCD. Thus, in this theoretical study, we will determine the effects of FCD, hence the osmotic pressure, on the confined-compression stress–relaxation behavior of cartilage using our mechano-electrochemical theory (Lai *et al.*, 1991). The objectives of this study are to determine the confined-compression stress–relaxation behavior of a charged, hydrated-soft tissues by: (1) delineating the contribution of the swelling pressure to the total stress when the tissue is compressed; and (2) determining the deformation, flow, pressure and electric fields in the tissue required for the understanding of mechano-electrochemical signal transduction within the tissue.

THEORY

In 1991, Lai and co-workers developed a mechano-electrochemical theory (the triphasic theory) for a charged, hydrated soft tissue based on the continuum mixture theory of Truesdell and Noll (1965) and Bowen (1980). (The reader may wish to refer to an excellent review article by de Boer (1996) on the development of poroelasticity theory and mixture

theory.) The triphasic theory evolved naturally from the biphasic theory for cartilage (Mow *et al.*, 1980) and the physicochemical theory for electrolyte solutions (Donnan, 1924; Friedman, 1986). In the theory, a charged hydrated soft tissue is modeled as a continuum mixture consisting of an incompressible solid phase (the ECM), an incompressible interstitial water phase, and an ion phase with two species (Na^+ and Cl^-). At each point within a tissue, macroscopically, the electroneutrality condition holds:

$$c^+ = c^- + c^F, \tag{1}$$

where c^+ is the Na^+ concentration, c^- is the Cl^- concentration, and c^F is the absolute value of the negative FCD on the solid phase. Note that all concentrations are per interstitial water volume. The motions of water and ions are governed by the following quasi-static momentum equations:

$$\text{water}\ \rho^w \nabla \mu^w = f_{ws}(v^s - v^w) + f_{w+}(v^+ - v^w) + f_{w-}(v^- - v^w), \tag{2}$$

$$\text{cation}\ \rho^+ \nabla \tilde{\mu}^+ = f_{+s}(v^s - v^+) + f_{+w}(v^w - v^+) + f_{+-}(v^- - v^+), \tag{3}$$

$$\text{anion}\ \rho^- \nabla \tilde{\mu}^- = f_{-s}(v^s - v^-) + f_{-w}(v^w - v^-) + f_{-+}(v^+ - v^-), \tag{4}$$

$$\text{tissue}\ \operatorname{div} \boldsymbol{\sigma} = \mathbf{0}, \tag{5}$$

where ρ^α and v^α denote the apparent density and the velocity of the α component ($\alpha = s, w, +, -$), respectively, with the indices s, w, +, − denoting quantities associated with solid, water, cation and anion, respectively. The quantities $\tilde{\mu}^+$ and $\tilde{\mu}^-$ are the electrochemical potentials for cations and anions, respectively, and μ^w is the chemical potential for water. Here, $f_{\alpha\beta}$'s are frictional coefficients (corresponding to resistance force per tissue volume) between the α and β components with $f_{\alpha\beta} = f_{\beta\alpha}$, and $\boldsymbol{\sigma}$ is the total stress tensor of the mixture. Equations (2)–(4) state that the driving force for the movement of water is the gradient of its chemical potential and the driving force for each of the ions is the gradient of its electrochemical potential. These driving forces are balanced by the frictional forces generated by the relative motions between the components, given by the terms $f_{\beta\alpha}(v^\alpha - v^\beta)$.

For an isotropic hydrated charged mixture with infinitesimal deformation, the constitutive equations of the triphasic theory are (see Lai *et al.*, 1991 and Gu *et al.*, 1998):

$$\sigma = -p\mathbf{I} + \lambda_s \operatorname{tr}(\mathbf{E})\mathbf{I} + 2\mu_s \mathbf{E}, \tag{6}$$

$$\mu^w = \mu_0^w + [p - RT\phi(c^+ + c^-) + B_w \operatorname{tr}(\mathbf{E})]/\rho_T^w, \tag{7}$$

$$\tilde{\mu}^+ = \mu_0^+ + (RT/M^+)\ln(\gamma_+ c^+) + F_c\psi/M^+, \tag{8}$$

$$\tilde{\mu}^- = \mu_0^- + (RT/M^-)\ln(\gamma_- c^-) - F_c\psi/M^-, \tag{9}$$

where p is the fluid pressure, $\mathbf{E}$ is the strain tensor measured from the reference configuration for the tissue equilibrated in a hypertonic salt bathing solution, λ_s and μ_s are Lamé coefficients of the solid matrix, μ_0^α is the reference chemical potential for phase α, M^+ and M^- are the molar weights of Na^+ and Cl^-, respectively, γ_+ and γ_- are the activity coefficients of Na^+ and Cl^-, respectively, ϕ is the osmotic coefficient, F_c is the Faraday constant, ψ is the electric potential, B_w is the coupling coefficient, and R and T are the universal gas constant and absolute temperature, respectively.

The continuity equations for each phase are

$$\partial\rho^\alpha/\partial t + \mathrm{div}(\rho^\alpha v^\alpha) = 0, \quad (\alpha = \mathrm{s}, \mathrm{w}, +, -) \tag{10}$$

where ρ^α, the apparent densities, are related to their true densities (ρ_T^α), and the volume fractions (φ^α) by $\rho^\alpha = \varphi^\alpha \rho_T^\alpha$ ($\alpha = \mathrm{s}, \mathrm{w}, +, -$). Note that

$$\Sigma\varphi^\alpha = 1, \quad (\text{summation over } \alpha = \mathrm{s}, \mathrm{w}, +, -) \tag{11}$$

for immiscible mixtures. For Na^+ and Cl^- ions, φ^+ and φ^- are negligible when compared with φ^w and φ^s, so that equation (11) can be approximated by

$$\varphi^s + \varphi^w = 1. \tag{12}$$

The apparent densities for ions are related to their concentrations by

$$\rho^+ = \varphi^w M^+ c^+ \quad \text{and} \quad \rho^- = \varphi^w M^- c^-. \tag{13}$$

1-D COMPRESSION STRESS RELAXATION PROBLEM

Figure 2(a) is the schematic representation of the problem under consideration. A cylindrical disc of tissue (thickness h), equilibrated in 0.15 M NaCl bath, is placed inside a confining cylinder prior to the application of an applied load. At $t = 0$, the porous–permeable loading platen acting on the (top) surface of the tissue is displaced with a constant velocity V_0 (Fig. 2(b)) until time t_0, beyond which, the platen is kept at a fixed position, while the specimen undergoes stress relaxation to the final equilibrium configuration.

The solution of this ramp–displacement relaxation problem using the biphasic formulation was first provided by Mow and coworkers (1980) under the assumption of infinitesimal deformation and constant permeability. Subsequently, biphasic formulations and solutions including strain-dependent permeability and/or finite deformations have been given (e.g., Ateshian *et al.*, 1997; Holmes *et al.*, 1985; Lai *et al.*, 1981). None of the above studies includes explicitly the fixed charges, although its effect is implicitly included in the aggregate modulus and permeability. In this study, we use the triphasic theory to determine explicitly the effects of the FCD on the stress–relaxation behavior of charged, hydrated-soft tissues. Our specific aims are: (1) to assess the contribution of the osmotic pressure effect to the relaxation behavior and to the aggregate modulus; and (2) to determine the effect of FCD on the peak stress of the experiment, and calculate the deformation and flow fields within the tissue. The relation between permeability and FCD was derived by Gu *et al.* (1993).

Reference configuration

We shall assume that in the initial ($t = 0$) state, at equilibrium, there is neither a mechanical load applied onto the porous platen (surface, $z = h$) nor any confining stress at the circumference of the testing specimen from the impermeable confining cylinder. However, the tissue is in a swollen state with a strain $e'_{zz}(z, 0)$ relative to the hypertonic configuration, and there is an osmotic pressure p'. In this initial equilibrium state for a homogeneous medium, the momentum equations show that σ, μ^w, $\tilde{\mu}^+$, $\tilde{\mu}^-$ are all constant through the depth of the tissue. The constants are determined from the boundary conditions $\sigma = 0$, $\mu^w = \mu^{w*}$, $\tilde{\mu}^+ = \tilde{\mu}^{+*}$, $\tilde{\mu}^- = \tilde{\mu}^{-*}$, where * quantities are associated with the external bathing NaCl solution. Thus, using the constitutive eqns (6)–(9) for both the tissue and the solution (where, for the external bathing solution, FCD, strain and pressure must all be set equal to zero), one can easily obtain (Lai *et al.*, 1991).

$$e'_{zz}(z,0) = \frac{RT[2\phi c^+(0) - \phi c^F(0) - 2\phi^* c^*(0)]}{H_\alpha} \tag{14}$$

$$p' = RT[2\phi c^+(0) - 2\phi^* c^*(0) - \phi c^F(0)] - B_w e'_{zz} \tag{15}$$

where

$$H_a = \lambda_s + 2\mu_s + B_w \tag{16}$$

and $c^+(0)$ is the Na^+ concentration at this initial swollen state, given by

$$c^+(z,0) = [c^F(0) + \sqrt{\{c^F(0)\}^2 + 4(\gamma^*_\pm/\gamma_\pm)^2 c^{*2}(0)}]/2, \tag{17}$$

where $c^F(0)$ is the FCD in the tissue and $c^*(0)$ is the NaCl concentration in the bath in this initial state. Since the tissue is assumed to be homogeneous, then $c^F(0)$ is a constant, and as a consequence the free swelling strain e'_{zz} is also a constant. In the following, we shall take this initial state as the reference state for the solid displacement $u^s(z,t)$. With reference to the hypertonic state, the displacement $u'^s(z,t)$ is given by

$$u'^s(z,t) = u^s(z,t) + u'^s(z,0) \tag{18}$$

from which, we have $e'_{zz}(z,t) = e_{zz}(z,t) + e'_{zz}(z,0)$ and

$$\frac{\partial e'_{zz}}{\partial z} = \frac{\partial e_{zz}}{\partial z}. \tag{19}$$

Governing equations

For this 1-D problem, all dependent variables are functions of the coordinate z and time t only (Fig. 2). We shall formulate this problem in terms of two coupled nonlinear partial differential equations for the solid displacement $u^s(z,t)$ and cation concentration $c^+(z,t)$. First, in terms of φ^w, c^+ and c^-, the continuity equations can be written as:

$$\frac{\partial \varphi^w}{\partial t} + \frac{\partial(\varphi^w v^w)}{\partial z} = 0, \tag{20}$$

$$\frac{\partial \varphi^w}{\partial t} - \frac{\partial v^s}{\partial z} + \frac{\partial(\varphi^w v^s)}{\partial z} = 0, \tag{21}$$

$$\frac{\partial(\varphi^w c^+)}{\partial t} + \frac{\partial(\varphi^w v^+ c^+)}{\partial z} = 0, \tag{22}$$

and

$$\frac{\partial(\varphi^w c^-)}{\partial t} + \frac{\partial(\varphi^w v^- c^-)}{\partial z} = 0, \tag{23}$$

Now, from eqns (20) and (21), we obtain an equation for v^s:

$$\frac{\partial v^s}{\partial z} = \frac{\partial}{\partial z}[\varphi^w(v^s - v^w)]. \tag{24}$$

Since the velocities v^s and v^w are zero at $z = 0$ for all time, the integration of the above equation with respect to z gives

$$v^s = \varphi^w(v^s - v^w). \tag{25}$$

For small displacement, $v^s = \partial u^s/\partial t$, therefore, eqns (25) can also be written as

$$\frac{\partial u^s}{\partial t} = \varphi^w(v^s - v^w). \tag{26}$$

Similarly, from eqns (20) and (22), we can obtain an equation for c^+:

$$\frac{\partial c^+}{\partial t} + v^w \frac{\partial c^+}{\partial z} = \frac{1}{\varphi^w}\frac{\partial}{\partial z}[c^+\varphi^w(v^w - v^+)]. \tag{27}$$

From the momentum eqns (2)–(4), the relative velocities $v^w - v^+$ and $v^s - v^w$ on the right side of the above two equations can be expressed in terms of the chemical and electrochemical potentials. Neglecting the frictional coefficients f_{+s}, f_{-s} and f_{+-}, we have,

$$v^w - v^+ = \frac{\rho^+}{f_{+w}}\frac{\partial \tilde{\mu}^+}{\partial z}, \tag{28}$$

$$v^s - v^w = \frac{1}{f_{ws}}\left[\rho^w \frac{\partial \mu^w}{\partial z} + \rho^+ \frac{\partial \tilde{\mu}^+}{\partial z} + \rho^- \frac{\partial \tilde{\mu}^-}{\partial z}\right], \tag{29}$$

$$v^s - v^+ = (v^s - v^w) + (v^w - v^+), \tag{30}$$

$$v^s - v^- = (v^s - v^w) + (v^w - v^-). \tag{31}$$

By inserting the constitutive eqns (6)–(9) into the above equations and using the following relation (from $\operatorname{div}\sigma = 0$)

$$\frac{\partial p}{\partial z} = (\lambda_s + 2\mu_s)\frac{\partial e'_{zz}}{\partial z} = (\lambda_s + 2\mu_s)\frac{\partial e_{zz}}{\partial z}, \tag{32}$$

we obtain

$$(v^s - v^w) = \frac{(\varphi^w)}{f_{ws}}\left(H_a \frac{\partial e_{zz}}{\partial z} + F_c c^F \frac{\partial \psi}{\partial z}\right) + \frac{\varphi^w RT}{f_{ws}} A(\gamma, \phi), \tag{33}$$

and

$$v^w - v^+ = \frac{(\varphi^w)}{f_{+w}}\left(RT\frac{1}{\gamma_+}\frac{\partial}{\partial z}(\gamma_+ c^+) + F_c c^+ \frac{\partial \psi}{\partial z}\right), \tag{34}$$

$$v^w - v^- = \frac{(\varphi^w)}{f_{-w}}\left(RT\frac{1}{\gamma_-}\frac{\partial}{\partial z}(\gamma_- c^-) - F_c c^- \frac{\partial \psi}{\partial z}\right) \tag{35}$$

where

$$A(\gamma,\phi)=\left[\frac{\partial}{\partial z}(c^{+}+c^{-}-\phi c^{+}-\phi c^{-})+\frac{c^{+}}{\gamma_{+}}\frac{\partial\gamma_{+}}{\partial z}+\frac{c^{-}}{\gamma_{-}}\frac{\partial\gamma_{-}}{\partial z}\right]. \tag{36}$$

We note that for ideal behaviors, the activity and osmotic coefficients are given by $\gamma_{+}=\gamma_{-}=\phi=1$, so that $A()=0$.

Using eqns (33) and (34), eqns (26) and (27) become:

$$\frac{\partial u_{s}}{\partial t}=\varphi^{w}(v^{s}-v^{w})=\left[\frac{(\varphi^{w})^{2}}{f_{ws}}\left(H_{a}\frac{\partial e_{zz}}{\partial z}+F_{c}c^{F}\frac{\partial\psi}{\partial z}\right)+\frac{(\varphi^{w})^{2}RT}{f_{ws}}A(\gamma,\phi)\right] \tag{37}$$

$$\frac{\partial c^{+}}{\partial t}+v^{w}\frac{\partial c^{+}}{\partial z}=\frac{1}{\varphi^{w}}\frac{\partial}{\partial z}[c^{+}\varphi^{w}(v^{w}-v^{+})]$$

$$=\frac{1}{\varphi^{w}}\frac{\partial}{\partial z}\left[\frac{c^{+}(\varphi^{w})^{2}}{f_{+w}}\left(RT\frac{1}{\gamma_{+}}\frac{\partial}{\partial z}(\gamma_{+}c^{+})+F_{c}c^{+}\frac{\partial\psi}{\partial z}\right)\right]. \tag{38}$$

Let the current density be denoted by I:

$$I=F_{c}\varphi^{w}[c^{+}(v^{+}-v^{s})-c^{-}(v^{-}-v^{s})]. \tag{39}$$

Using eqns (30), (31), (33) and (34), we obtain

$$I=-F_{c}\varphi^{w}\left[\frac{D_{F}}{RT}H_{a}\frac{\partial e_{zz}}{\partial z}+D_{F}A(\gamma,\phi)+\frac{D_{+}}{\gamma_{+}}\frac{\partial}{\partial z}(\gamma_{+}c^{+})-\frac{D_{-}}{\gamma_{-}}\frac{\partial}{\partial z}(\gamma_{-}c^{-})+\frac{F_{c}}{RT}\alpha\frac{\partial\psi}{\partial z}\right] \tag{40}$$

where

$$\alpha=D_{F}c^{F}+D_{+}c^{+}+D_{-}c^{-}. \tag{41}$$

$$D_{F}=\frac{c^{F}\varphi^{w}RT}{f_{ws}},\quad D_{+}=\frac{c^{+}\varphi^{w}RT}{f_{w+}},\quad D_{-}=\frac{c^{-}\varphi^{w}RT}{f_{w-}}. \tag{42}$$

In the following, we will consider only the case where $I=0$ (i.e., the open circuit case). For this case,

$$\alpha\frac{\partial\psi}{\partial z}=\frac{RT}{F_{c}}\left[\frac{D_{-}}{\gamma_{-}}\frac{\partial}{\partial z}(\gamma_{-}c^{-})-\frac{D_{+}}{\gamma_{+}}\frac{\partial}{\partial z}(\gamma_{+}c^{+})-D_{F}A(\gamma,\phi)\right]-\frac{D_{F}}{F_{c}}\left[H_{a}\frac{\partial e_{zz}}{\partial z}\right]. \tag{43}$$

Substituting the expression for $\partial\psi/\partial z$ in eqns (33) and (34), we obtain:

$$v^{s}-v^{w}=\frac{1}{\alpha}\left[\frac{D_{+}c^{+}+D_{-}c^{-}}{K}\left(H_{a}\frac{\partial^{2}u^{s}}{\partial z^{2}}\right)-D^{F}\left(\frac{D_{+}}{\gamma_{+}}\frac{\partial\gamma_{+}c^{+}}{\partial z}-\frac{D_{-}}{\gamma_{-}}\frac{\partial\gamma_{-}c^{-}}{\partial z}\right)\right]$$

$$+\frac{D_{F}(D_{+}c^{+}+D_{-}c^{-})}{c^{F}\alpha}A(\gamma,\phi) \tag{44}$$

$$(v^{w}-v^{+})=\left[\frac{D_{+}}{c^{+}\alpha}\left(\frac{D_{-}c^{+}}{\gamma_{-}}\frac{\partial\gamma_{-}c^{-}}{\partial z}+(D_{-}c^{-}+D_{F}c^{F})\frac{1}{\gamma_{+}}\frac{\partial\gamma_{+}c^{+}}{\partial z}-c^{+}D_{F}A(\gamma,\phi)\right)\right.$$

$$\left.-\frac{c^{F}D_{+}}{\alpha K}\left(H_{a}\frac{\partial^{2}u^{s}}{\partial z^{2}}\right)\right] \tag{45}$$

where $K = f_{ws}/\phi^w$. An equation for $v^w - v^-$ can be similarly obtained. Thus, in the absence of an electric current, we have

$$\frac{\partial u^s}{\partial t} = \frac{\varphi^w}{\alpha}\left[\frac{D_+c^+ + D_-c^-}{K}\left(H_a\frac{\partial^2 u^s}{\partial z^2}\right) - D^F\left(\frac{D_+}{\gamma_+}\frac{\partial \gamma_+ c^+}{\partial z} - \frac{D_-}{\gamma_-}\frac{\partial \gamma_- c^-}{\partial z}\right)\right] + \frac{\varphi^w D_F(D_+c^+ + D_-c^-)}{\partial c^F}A(\gamma,\phi) \quad (46)$$

$$\frac{\partial c^+}{\partial t} + v^w\frac{\partial c^+}{\partial z} = \frac{1}{\varphi^w}\frac{\partial}{\partial z}\left[\frac{\varphi^w D_+}{\alpha}\left(\frac{D_-c^+}{\gamma_-}\frac{\partial \gamma_- c^-}{\partial z} + (D_-c^- + D_F c^F)\frac{1}{\gamma_+}\frac{\partial \gamma_+ c^+}{\partial z} - c^+ D_F A(\gamma,\phi)\right) - \frac{c^F\varphi^w D_+ c^+}{\alpha K}\left(H_a\frac{\partial^2 u^s}{\partial z^2}\right)\right] \quad (47)$$

where $v^w = (1 - 1/\varphi^w)\partial u^s/\partial t$. With φ_0^W and $c^F(0)$ denoting the water volume fraction and FCD at $t = 0$, respectively, we note that

$$\varphi^w = \varphi_0^w + (1-\varphi_0^w)e \quad \text{and} \quad c^F = c_0^F(0)(1 - e/\varphi_0^w),$$

where e is the dilatation of the solid matrix.

We note that for ideal behaviors, $\phi = \gamma_+ = \gamma_- = 1$, the above equations simplify to

$$\frac{\partial u^s}{\partial t} = \varphi^w\left[\frac{H_a}{K}\frac{D^+c^+ + D^-c^-}{\alpha}\frac{\partial^2 u^s}{\partial z^2} - \frac{D^F}{\alpha}\left(D^+\frac{\partial c^+}{\partial z} - D^-\frac{\partial c^-}{\partial z}\right)\right], \quad (48)$$

$$\frac{\partial c^+}{\partial t} + v^w\frac{\partial c^+}{\partial z} = \frac{1}{\varphi^w}\frac{\partial}{\partial z}\left[\frac{\varphi^w D_+}{\alpha}\left(D_-c^+\frac{\partial c^-}{\partial z} + (D_-c^- + D_F c^F)\frac{\partial c^+}{\partial z}\right) - \frac{c^F\varphi^w D_+ c^+}{\alpha K}\left(H_a\frac{\partial^2 u^s}{\partial z^2}\right)\right]. \quad (49)$$

Following the general formulation of the initial and boundary conditions, the numerical solution for this ideal case will be provided below.

Initial conditions

Before the application of the ramp displacement, the charged-hydrated tissue sample (Fig. 2(a)) is equilibrated in a NaCl solution of concentration c^* (e.g., 0.15 M), and is in a swollen state relative to our hypertonic reference configuration. As mentioned earlier, we shall take this swollen state as the reference configuration for the solid displacement in the stress–relaxation problem. Thus, the initial conditions are:

$$u^s(z,0) = 0 \quad (50)$$

and

$$c^+(z,0) = [c^F(0) + \sqrt{\{c^F(0)\}^2 + 4(\gamma_\pm^*/\gamma_\pm)^2 c^{*2}(0)}]/2, \quad (51)$$

where $c^F(0)$ is the FCD at $t = 0$ (the initial swollen state).

Boundary conditions

The bottom surface ($z = 0$) is assumed to be rigid, therefore,

$$u^s(0, t) = 0 \quad \text{at } z = 0. \tag{52}$$

Also, the boundary is assumed to be impermeable to water and ions, i.e., the velocity components (v^s, v^+, v^- and v^w) are zero. It follows from the momentum equations that at this boundary,

$$\frac{\partial \mu^w}{\partial z} = \frac{\partial \tilde{\mu}^+}{\partial z} = \frac{\partial \tilde{u}^-}{\partial z} = 0. \tag{53}$$

Using the constitutive equations for the chemical and electrochemical potentials, the above equations can be shown to lead to the following boundary conditions for c^+ at $z = 0$:

$$\frac{\partial c^+}{\partial z} = 0. \tag{54}$$

In fact, at this boundary all the following identities hold:

$$\frac{\partial c^+}{\partial z} = \frac{\partial c^-}{\partial z} = \frac{\partial e_{zz}}{\partial z} = \frac{\partial p}{\partial z} = \frac{\partial \psi}{\partial z} = 0. \tag{55}$$

The upper surface of the tissue is at $z = h$, where a ramp displacement $U(t)$ is imposed via a rigid porous–permeable loading platen. Thus, at this surface (i.e., $z = h$), we have:

$$u^s(h, t) = -U(t), \tag{56}$$

where

$$U(t) = V_0 t \quad \text{for } t \leqslant t_0 \quad \text{and} \quad U(t) = V_0 t_0 \quad \text{for} \quad t > t_0, \quad (V_0 > 0). \tag{57}$$

Also, the continuity of water chemical potential $\mu^w = \mu^{w*}$ at the platen–tissue interface gives

$$p(h, t) = RT[2\phi c^+(h, t) - 2\phi^* c^{+*}(h, t) - \phi c^F(h, t)] - B_w[e_{zz}(h, t) + e'_{zz}(h, 0)]. \tag{58}$$

Thus,

$$\sigma_{zz}(h, t) = -RT[2\phi c^+(h, t) - 2\phi^* c^{+*}(h, t) - \phi c^F(h, t)] + H_a[e_{zz}(h, t) + e'_{zz}(h, 0)] \tag{59}$$

where we recall e'_{zz} is the free-swelling strain relative to the hypertonic reference configuration. Letting P_A denote the total (mixture) compressive stress on the tissue surface ($z = h$) resulting from the prescribed ramp displacement, we obtain:

$$P_A = -H_a \frac{\partial u^s(z, t)}{\partial z}$$
$$+ RT[2\phi(c^+(h, t) - c^+(h, 0)) - \phi(c^F(h, t) - c^F(h, 0)) - 2\phi^*(c^{+*}(h, t) - c^{+*}(h, 0))] \tag{60}$$

where

$$c^+(h,t) = \text{constant} = [c^F(h,t) + \sqrt{c^{F2}(h,t) + 4(\gamma_\pm^*/\gamma_\pm)^2 c^{*2}}]/2.$$

In arriving at the above equation, we have used eqn (14) for e'_{zz}.

For simplicity, we shall assume in this paper that the external NaCl solution is well stirred so that its concentration remains constant throughout the loading process, i.e., we assume $c^{+*}(h,t) = c^{+*}(h,0)$ at all time. The interaction between the tissue and the bath will be dealt with in a separate paper.

RESULTS AND DISCUSSION

Numerical results are presented only for the ideal case where $\gamma_+ = \gamma_- = \phi = 1$. The nonlinear governing eqns (48) and (49) subject to the initial conditions (50) and (51) and boundary conditions (52) and (53) are solved numerically using a finite difference method. Once the distribution of the displacement of solid matrix and cation (Na^+) concentration within the tissue are obtained, all other quantities can be calculated from the above defining equations. For articular cartilage, the following physiologically realistic parameters are used in our numerical calculations:

$t_0 = 200$ s $\quad c^* = 0.15$ M, $\quad H_a = 0.3$ MPa,

$R = 8.314$ J/mol K, $\quad T = 298$ K, $\quad D^+ = 0.5 \times 10^{-9}$ m^2/s, $\quad D^- = 0.8 \times 10^{-9}$ m^2/s,

$K = 7.0 \times 10^{14}$ Ns/m^4, $\quad \phi_0^w = 0.75$, $\quad c_0^F = 0.20$ mEq/ml,

$V_0 = 0.25$ μm/s, $\quad h = 0.5$ mm.

Figures 3a and 3b show the strain distribution within the tissue at various times. The strains are monotonically varying with depth, always compressive, and the maximum value always occurs at the surface ($z = h$). During the compressive stage ($t < 200$ s), the compressive strain increases with time (Fig. 3a) until the end of the ramp ($t = 200$ s). During the relaxation stage ($t > 200$ s), the compressive strain at the surface decreases with time while the compressive strain at the bottom ($z = 0$) continues to increase (Fig. 3b) until a uniform equilibrium compressive strain of 10% is reached. We note that with a 10% surface to surface compressive strain applied across the surfaces in 200 s, due to drag-induced compaction (Lai and Mow, 1980), the local true compressive strain at the tissue surface reached up to 20% before decreasing to the final equilibrium value of 10%. The compressive strain at the bottom reached this same equilibrium value monotonically. This result is consistent with the biphasic analysis reported by Mow *et al.* (1980). Since the FCD

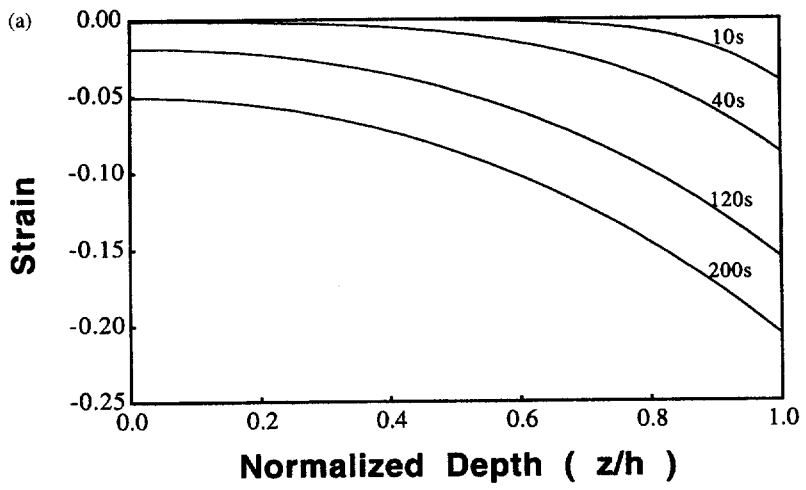

Fig. 3a. Strain distributions within the tissue at different times during the compression stage.

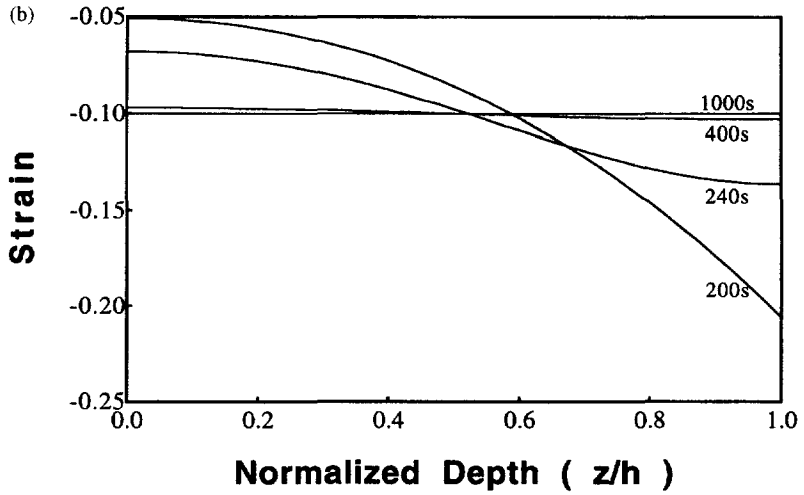

Fig. 3b. Strain distributions within the tissue during the stress–relaxation stage.

is a linear function of the strain (for this infinitesimal deformation formulation), the distributions of FCD in the compressive stage and relaxation stage follow similar patterns to those of the compressive strain distribution, see Figs 4a and 4b.

Figures 5a and 5b show the nonlinear distributions of Na^+ concentration within the tissue at various times. During the compression stage ($t \leqslant 200$ s; Fig. 5a), the Na^+ concentration increases with time, and is particularly accentuated near the surface ($z = h$). This is due to the compaction effect (with significant compressive strain) which increases the FCD, and thereby requires more positive counter-ions (Na^+) to maintain electroneutrality. These increases are more pronounced near the surface where the local FCD is higher. During the relaxation stage ($t > 200$ s), redistribution of Na^+ concentration takes place within the tissue until an equilibrium is reached (Fig. 5b). Figures 6a and 6b provide the dependence of Cl^- concentrations as a function of depth and time. Note that the increase in FCD will decrease the Cl^- concentration. This phenomenon is known as Donnan exclusion effect (Donnan, 1924).

Figure 7 shows the history of total compressive stress $P_A(t)$ corresponding to the history of the prescribed surface displacement. Also shown in the same figure are the histories of the fluid pressure at $z = 0$ (impermeable interface) and at $z = h$ (porous–permeable interface). We note that the fluid pressure curves follow the same pattern as the

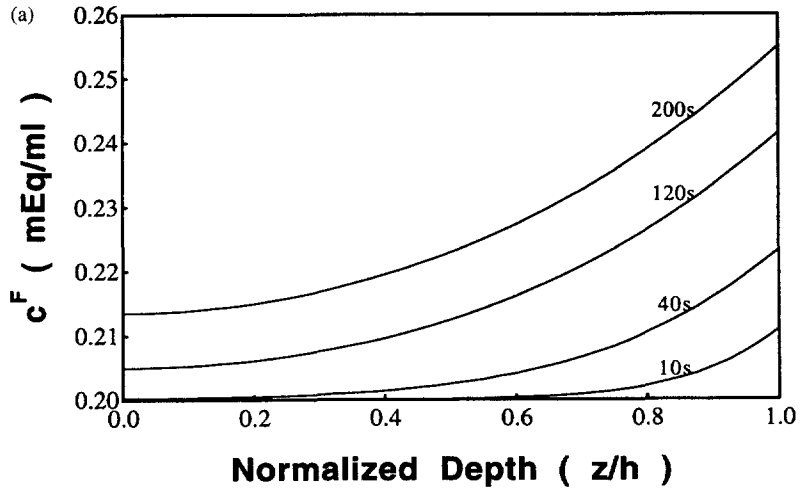

Fig. 4a. Calculated FCD distribution as a function of time during the compression stage.

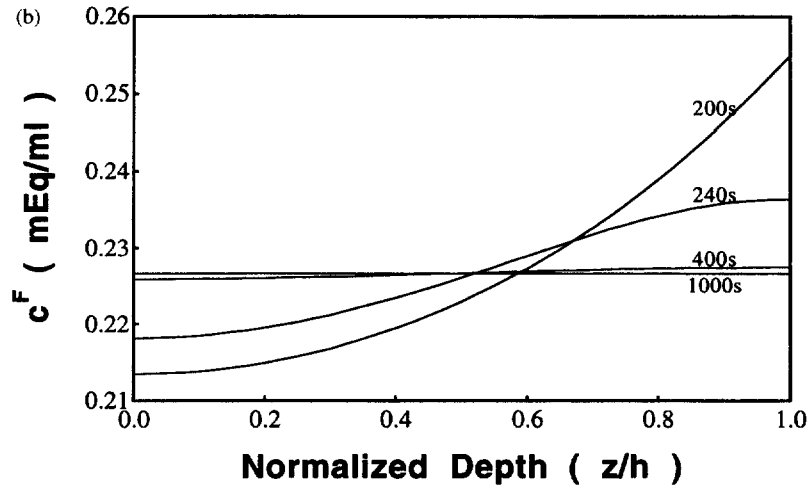

Fig. 4b. Calculated FCD distribution as a function of time during the stress–relaxation stage.

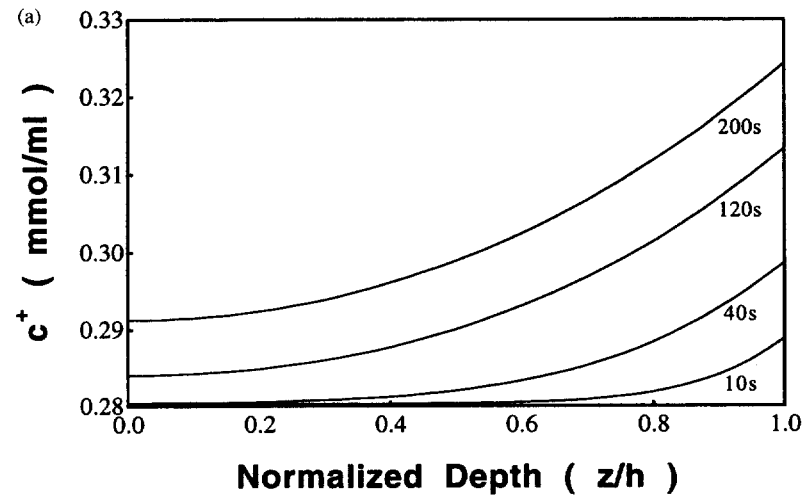

Fig. 5a. Na^+ concentration distributions at different times during the compression stage.

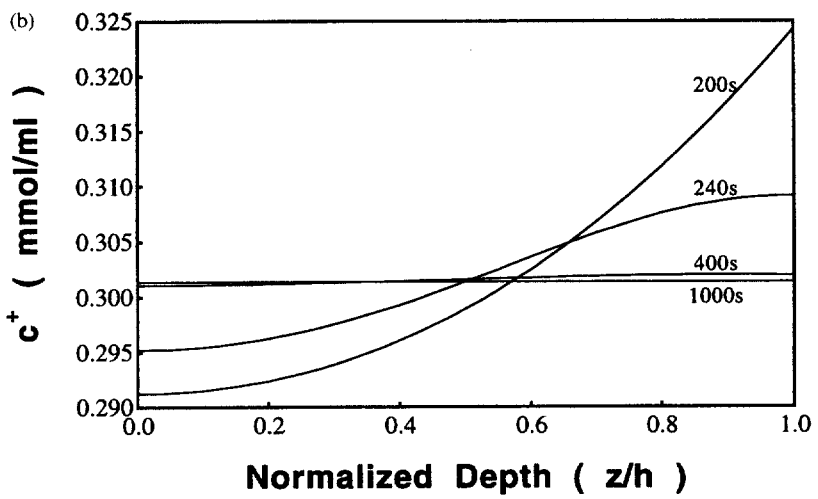

Fig. 5b. Na^+ concentration distributions at different times during the stress–relaxation stage.

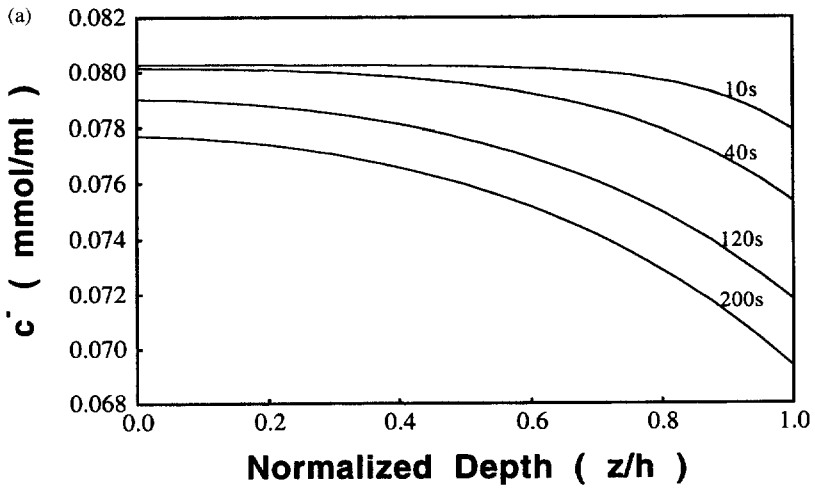

Fig. 6a. Cl^- concentration distributions at different times during the compression stage.

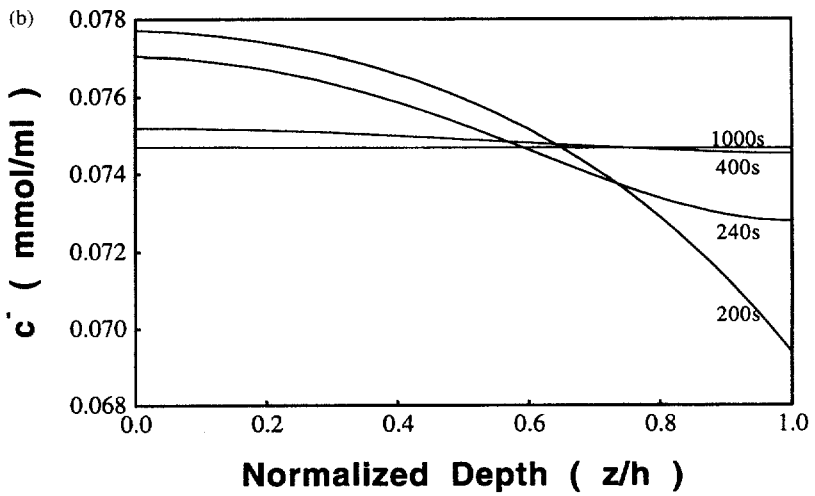

Fig. 6b. Cl^- concentration distributions at different times during the stress–relaxation stage.

applied loading curve, $P_A(t)$, reaching peak values at the end of the ramp stage and relaxing to an equilibrium value at large time. This equilibrium fluid pressure, which is uniform throughout the depth, is the Donnan osmotic pressure frequently reported in the literature (e.g., Maroudas, 1979). Clearly, we see from this figure that at equilibrium, approximately one half of the load support is from the Donnan osmotic pressure. During the transient stage, in addition to the Donnan osmotic effect, there is also the fluid pressurization effect, due to flow resistance of the solid matrix. We note that this latter effect always exists even if there is no FCD. From the fluid pressure curve at $z = 0$ (the impermeable bottom boundary) we see that during the compressive stage, more than 90% of load support at this depth is from fluid pressure. This is because the solid matrix strains are small at this depth during the compressive stage. On the other hand, at $z = h$ (the porous–permeable interface), there are larger solid matrix compressive strains during the same stage and therefore, the contribution to load support from fluid pressure is smaller than that at the bottom-dashed curve in this figure.

If we curvefit the loading history of $P_A(t)$ (i.e., Fig. 7 obtained from the triphasic theory), with the biphasic theory to determine the equivalent aggregate modulus H_A and the equivalent diffusive resistance coefficient K_{ws} (which is related to the permeability k by the relation $K_{ws} = k/(\phi^w)^2$), we obtain the result shown in Fig. 8. We see that, insofar as

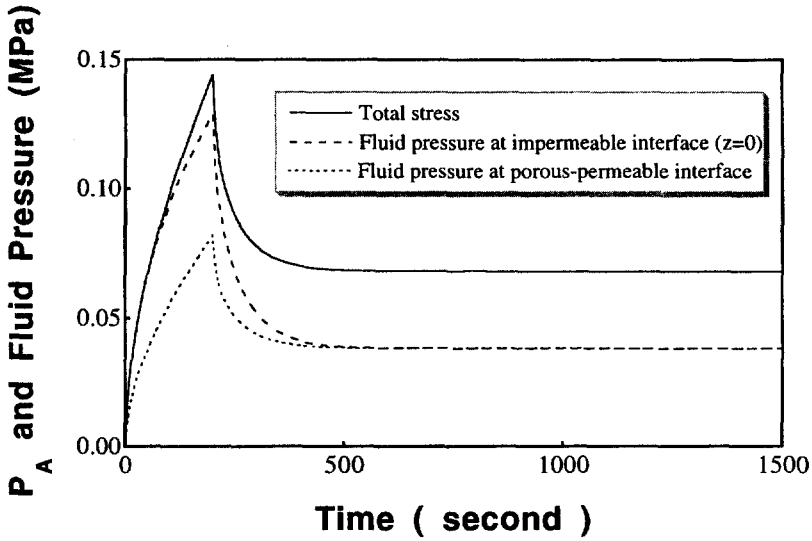

Fig. 7. Total compressive stress and fluid pressure at $z = 0$ and at $z = h$. The fluid pressure at the impermeable interface ($z = 0$) supports more than 90% of the applied load during the compression stage. At equilibrium, the fluid pressures at both the porous interface ($z = h$) and the impermeable interface ($z = 0$) reach the Donnan osmotic pressure.

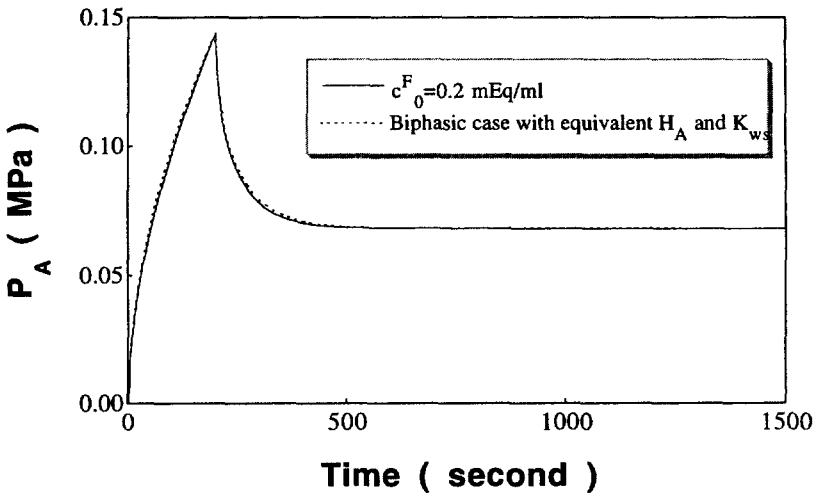

Fig. 8. Total compressive stress as a function of time predicted by the triphasic theory ($c_0^F = 0.2$ mEq/ml) and the biphasic theory with equivalent aggregate modulus (H_A) and equivalent diffusive resistance coefficient (K_{ws}).

the outward manifestation of the stress relaxation behavior is concerned (as characterized by the loading history P_A), both theories, the biphasic and the triphasic, can describe the same behavior with little difference. However, the two theories predict different fluid pressure histories inside the tissue as shown in Fig. 9. The fluid pressure relaxes to zero in the biphasic theory whereas the fluid pressure relaxes to the Donnan osmotic pressure in the triphasic theory. The equivalent aggregate modulus, as determined from the curvefit, gives a value of $H_A = 0.683$ MPa, which is a little more than twice the value of the triphasic intrinsic modulus H_a of 0.3 MPa used in the calculation for the triphasic medium, and the equivalent diffusive resistance coefficient K_{ws} of 1.02×10^{15} Ns/m^4 as compared with the triphasic frictional coefficients f_{ws} of 5.25×10^{14} Ns/m^4. These equivalent values of H_A and diffusive resistance coefficient K_{ws} embody the FCD effect in the biphasic theory which does not have a FCD.

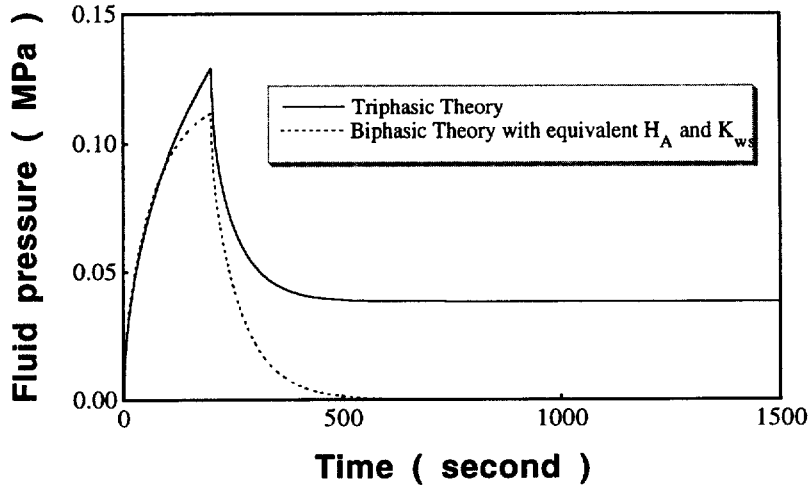

Fig. 9. Comparison of fluid pressures calculated by the triphasic and biphasic theories, at the impermeable interface ($z = 0$). The biphasic pressure does not include the FCD (osmotic) effect.

It is interesting to note that in the biphasic theory, continuity conditions require that the interstitial fluid pressure at a cartilage boundary (e.g., the dotted curve in Fig. 9) be equal to the external fluid pressure in the adjacent bath. Indeed, this has been confirmed experimentally that the fluid pressure measured immediately outside of the cartilage agrees very well with theoretical predictions of the biphasic theory, in the configurations of confined compression creep and stress–relaxation (Soltz and Ateshian, 1997, 1998). It is evident, however, that simply placing a pressure transducer against the surface of cartilage cannot produce measurements of the osmotic contributions to the interstitial fluid pressure as predicted by the triphasic theory (Fig. 9). It remains an experimental challenge at this time to perform measurements of the transient cartilage interstitial fluid pressure inclusive of osmotic effects.

It is important to note that while the triphasic theory reduces to the biphasic theory when the FCD is zero, the elastic modulus (λ_s and μ_s) and the diffusive resistance coefficient (K_{ws}) in the biphasic theory are in general, not the same as those in the triphasic theory. They have been determined from experiments in such a way that the aggregate modulus and the diffusive resistance coefficient include implicitly all the FCD (including osmotic) effects.

Finally, Fig. 10 shows that the peak stress, at the end of the compression stage ($t = t_0$), increases nonlinearly with the FCD. In the normal physiologic range of c^F for articular cartilage, 0.1–0.4 mEq/ml, we see an added benefit of the proteoglycan charge groups. It enhances the ability of the tissue to support higher loads in a dynamically loaded situation. Clearly, in osteoarthritic cartilage, when the proteoglycans are depleted, this important beneficial effect is negated.

CONCLUSIONS

A special case of the general mechano-electrochemical theory developed by Lai and co-workers (1991) was used to solve the confined compression stress relaxation problem. A pair of nonlinear coupled partial differential equations governing the displacement component of solid matrix (u^s) and cation concentration (c^+) were derived to describe the stress relaxation experiment. The initial-boundary value problem is solved using the finite difference method. Using physiologic data available in the literature, it was found that: (1) Donnan osmotic pressure and intrinsic matrix stiffness contribute in nearly equal proportion to the load support at equilibrium: (2) for the rate of compression of 10% in 200 sec, during the compression stage, the fluid pressure at the impermeable boundary supports nearly all the load, whereas near the porous–permeable interface, the fluid pressure only

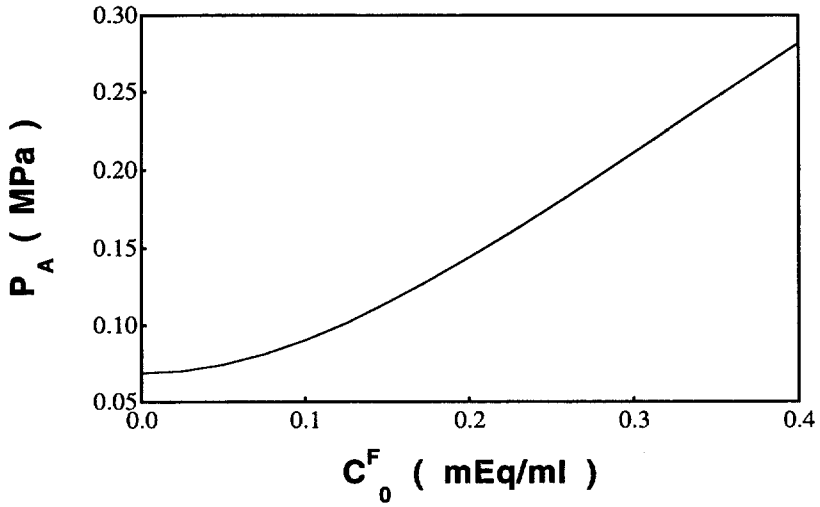

Fig. 10. Peak value of total compressive stress as a function of fixed charge density (c_0^F).

partially supports the load; (3) equivalent aggregate modulus and equivalent diffusive resistance coefficient can be found for a biphasic medium which predicts the same stress relaxation behavior. These equivalent parameters for the biphasic model embody the FCD effects of the triphasic medium. However, the internal fluid pressures predicted by the two models are different; and (4) the FCD accentuates the peak stress response found at the end of the compression stage thus providing enhanced load support for cartilage having a normal physiologic range of proteoglycans.

Acknowledgements—This work was supported in part by grants from the NIH (AR 41913) and the OREF (96-043). The authors wish to thank Mr Dongning Sun and Mr Chanbin Wang for their assistance in the preparation of this manuscript.

REFERENCES

Akizuki, S., Mow, V. C., Muller, F., Pita, J. C., Howell, D. S. and Manicourt, D. H. (1986) The tensile properties of human knee joint cartilage I: influence of ionic conditions, weight bearing, and fibrillation on the tensile modulus. *J. Orthop. Res.* **4,** 379–392.

Ateshian, G. A., Warden, W. H., Kim, J. J., Grelsamer, R. P. and Mow, V. C. (1997) Finite deformation biphasic material properties of bovine articular cartilage from confined compression experiments. *Journal of Biomechanics* **30,** 1157–1164.

Biot, M. A. (1941) General theory of three-dimensional consolidation. *Journal of Applied Physics* **12,** 155–164.

Bowen, R. M. (1980) Incompressible porous media models by use of the theory of mixtures. *International Journal of Engineering Science* **18,** 1129–1148.

Buschmann, M. D. and Grodzinsky, A. J. (1995) A molecular model of proteoglycan-associated electrostatic forces in cartilage mechanics. *ASME J. Biomech. Engng* **17,** 179–192.

deBoer, R. (1996) Highlights in the historical development of the porous media theory: toward a consistent macroscopic theory. *Applied Mechanics Review* **49,** 201–262.

Donnan, F. G. (1924) The theory of membrane equilibria. *Chemical Review* **1,** 73–90.

Eisenberg, S. R. and Grodzinsky, A. J. (1987) The kinetics of chemically induced nonequilibrium swelling of articular cartilage and corneal stroma. *ASME J. Biomech. Engng* **109,** 79–89.

Frank, E. H. and Grodzinsky, A. J. (1987) Cartilage electromechanics—II. A continuum model of cartilage electrokinetics and correlation with experiments. *Journal of Biomechanics* **20,** 629–639.

Friedman, M. H. (1986) *Principles and Models of Biological Transport.* Springer-Verlag, Berlin, Heidelberg, New York, Tokyo.

Grodzinsky, A. J., Lipshitz, H. and Glimcher, M. J. (1978) Electromechanical properties of articular cartilage during compressive stress relaxation. *Nature* **275,** 448–450.

Gu, W. Y., Lai, W. M. and Mow, V. C. (1993) Transport of fluid and ions through a porous-permeable charged-hydrated tissue, and streaming potential data on normal bovine articular cartilage. *Journal of Biomechanics* **26,** 709–723.

Gu, W. Y., Lai, W. M. and Mow, V. C. (1995) Effects of mechanical stress and deformation on passive ion transport through hydrated permeable tissues. *Ann. Biomed. Engng* **23,** 104.

Gu, W. Y., Lai, W. M. and Mow, V. C. (1997) A triphasic analysis of negative osmotic flow through charged-hydrated soft tissues. *Journal of Biomechanics* **30,** 71–78.

Gu, W. Y., Lai, W. M. and Mow, V. C. (1998) A mixture theory for charged hydrated soft tissues containing multi-electrolytes: Passive transport and swelling behaviors. *J. Biomech. Engng* **120**(2), 169–180.

Hardingham, T. E. and Fosang, A. (1992) Proteoglycans: many forms and many functions. *FASEB Journal* **10,** 143–183.

Holmes, M. H., Lai, W. M. and Mow, V. C. (1985) Singular perturbation analysis of the nonlinear, flow-dependent, compressive stress–relaxation behavior of articular cartilage. *ASME J. Biomech. Engng* **103,** 61–66.

Katchalsky, A. (1971) Polyelectrolytes. *Pure Appl. Chem.* **26,** 327–373.

Katchalsky, A. and Curran, P. F. (1975) *Nonequilibrium Thermodynamics in Biophysics*, 4th edn. Harvard University Press, Cambridge, MA.

Lai, W. M. and Mow, V. C. (1980) Drag-induced compaction of articular cartilage during a permeation experiment. *Biorheology* **17,** 111–123.

Lai, W. M., Gu, W. and Mow, V. C. (1994) Flows of electrolytes through charged hydrated biologic tissue. *Applied Mechanics Review* **47,** 277–281.

Lai, W. M., Hou, J. S. and Mow, V. C. (1991) A triphasic theory for the swelling and deformation behaviors of articular cartilage. *ASME J. Biomech. Engng* **13,** 245–258.

Lai, W. M., Mow, V. C. and Roth, V. (1981) Effects of nonlinear strain-dependent permeability and rate of compression on the stress behavior of articular cartilage. *ASME J. Biomech. Engng* **103,** 61–66.

Maroudas, A. (1979) Physiochemical properties of articular cartilage. In: *Adult Articular Cartilage*, ed. M. A. R. Freeman. pp. 215–290. Pitman Medical, Kent, U.K.

Mow, V. C., Ratcliffe, A. and Poole, A. R. (1992) Cartilage and diarhrodial joints as paradigms for hierarchical materials and structure. *Biomaterials* **13,** 67–97.

Mow, V. C., Kuei, S. C., Lai, W. M. and Armstrong, C. G. (1980) Biphasic creep and stress relaxation of articular cartilage in compression: theory and experiments. *ASME J. Biomech. Engng* **102,** 73–84.

Muir, H. (1983) Proteoglycans as organisers of the intercellular matrix. *Biochem. Soc. Trans.* **9,** 489–497.

Myers, E. R., Lai, W. M. and Mow, V. C. (1984) A continuum theory and an experiment for the ion-induced swelling behavior of articular cartilage. *ASME J. Biomech. Engng* **106,** 151–158.

Overbeek, J. Th. G. (1956) The Donnan equilibrium. *Prog. Biophys. Biophys. Chem.* **6,** 58–84.

Setton, L. A., Gu, W. Y., Lai, W. M. and Mow, V. C. (1995) Predictions of the swelling induced pre-stress in articular cartilage. In: *Mechanics of Poroelastic Media*, ed. A. P. S. Selvadurai, pp. 299–322. Kluwer Academic Publishers.

Soltz, M. A. and Ateshian, G. A. (1997) Experimental measurement of cartilage interstitial fluid pressurization under confined compression stress–relaxation. *Advances in Bioengineering. ASME, BED* **36,** 159–160.

Soltz, M. A. and Ateshian, G. A. (1998) Experimental verification and theoretical prediction of cartilage interstitial fluid pressurization at an impermeable contact interface in confined compression. *Journal of Biomechanics*, accepted.

Truesdell, C. and Noll, W. (1965) The non-linear field theories of mechanics. *Handbuch der Phyisk III*/3. Springer-Verlag, Berlin.